RATIONAL DESIGN AND DEVELOPMENT OF THE REGENERATIVE PUMP

by

DAVID P. DeWITT

B. S. M. E., Duke University
(1955)

SUBMITTED IN PARTIAL FULFILLMENT

OF THE REQUIREMENTS FOR THE DEGREE OF

MASTER OF SCIENCE IN MECHANICAL ENGINEERING

AT THE

MASSACHUSETTS INSTITUTE OF TECHNOLOGY

JANUARY 1957

Signature of Author: _____
Department of Mechanical Engineering, Jan. 14, 1957

Certified By: _____
Thesis Adviser

Accepted By: _____
Chairman, Departmental Committee of Graduate Students

ABSTRACT

RATIONAL DESIGN AND DEVELOPMENT OF
THE REGENERATIVE PUMP

by

David P. DeWitt

Submitted to the Department of Mechanical Engineering on January 14, 1957 in partial fulfillment of the requirements for the degree of Master of Science.

A theory of operation of the regenerative pump was presented several years ago based upon internal flow following helical streamlines. This theory postulates that there are two major losses occuring within the pump. A new pump was designed specifically to reduce one of these losses -- resistance to the internal circulatory flow. This investigation shows that improvements in internal efficiency and head rise were effected.

The geometry of the new pump is such that it was possible to insert fillers to induce the flow to follow well defined helical streamlines. Comparison of theoretical and experimental curves was reduced to the task of computing only two parameters, without an adjustment of a third as was previously required. The results of these tests have been used to predict performance curves of a new unit, "designed" to reduce the second major loss within the pump-blade entrance or shock loss.

Thesis Supervisor: W. A. Wilson

Title: Associate Professor of Mechanical Engineering

TABLE OF CONTENTS

LIST OF ILLUSTRATIONS

Figure No.

List of Symbols

g	acceleration of gravity
H	head in ft. of fluid pumped
k_c	circulatory flow coefficient
P	pressure
Q	volume rate of flow
L/D_h	length to hydraulic diameter ratio
u	internal energy in absence of. . . .
U	wheel speed
V	velocity
W	work input

DIMENSIONS

r	radius
r_g	radius to centroid of cross-section of channel
r_o	position of mean stream line leaving impeller passage
r_i	position of mean stream line entering impeller passage
b_o	radial length of circulatory flow area leaving impeller
b_i	radial length of circulatory flow area entering impeller
A	cross-sectional area of channel
D	diameter to cg of channel

GREEK SYMBOLS

α	V_{ti}/U_i
σ	V_{to}/U_o, slip factor

β	blade angle
ρ	density
τ	torque
ω	angular velocity
θ	angular measure from inlet, radians
θ_p	linear region of pump, radians
ψ	$\frac{Q}{Q_s}$, ratio of actual flow rate to solid body rotation of channel area
$\frac{d\psi}{d\theta}$	$\frac{gH}{\omega^2 D^2} \cdot \frac{1}{\theta_p}$, pressure coefficient
$\frac{dP}{d\theta}$	$\frac{g\tau}{\rho \omega^2 D^5} \cdot \frac{1}{\theta_p}$, power coefficient
η	$\frac{\rho Q H}{W}$, efficiency

SUBSCRIPTS

c	circulatory flow
s	solid body rotation
t	tangential direction

FOREWORD

The author's investigation concerns the latest developments in a research program started in September, 1952. The Worthington Corporation established a grant-in-aid at the Institute for the purpose of rationalizing the nature of the regenerative pumping process with a view to achieving improved performance.

The initial step in the program was to establish the kinematics of the fluid mechanism within the pump. A theory based on helical streamlines was postulated and data from a commercial pump was used to demonstrate the validity of the theory. A larger lucite "variable geometry" pump was designed and tested, and further light was shed on the nature of the pump mechanism. Some effects of geometry were established and ideas for improvement were generated. The pump tested in the author's investigation is the result.

The author wishes to acknowledge support for this project received from the Worthington Corporation. The author is indebted to Professors W. A. Wilson and M. A. Santalo for their advice and assistance based upon several years of experience with this project.

1. INTRODUCTION

The regenerative pump is a hydrodynamic unit which is referred to in the literature by various names including: turbine pump, periphery pump, friction pump, claw pump, and a host of other less descriptive names. The performance of a regenerative pump is unusual due to very low specific speeds and the inverse relation of head and power to capacity. The efficiency is not impressive, but when compared with units of similar specific speeds, the efficiency is quite acceptable. *

Regenerative pumps have found application in lubrication, filtering, control, and booster systems. More than ever there is a demand for low-flow, high-head pumps which is still to be satisfied. A regenerative pump is capable of replacing a 6 or 7 stage centrifugal compressor, so far as producing the required head. The advantage is the simplicity of design, assembly, and maintenance; but, the relatively poor efficiency is the decisive disadvantage.

There are several styles of pumps as shown in the sketches of Figure 2. The double bladed impeller (A) is the most common form of commercial unit. Impeller (B) is a "half" double bladed impeller or inverted "L" shaped channel used by Santalo[1]** and Senoo[2] for conducting tests here at the Institute. Impeller (C) is the shape used by the author in this present

---

* Fig. 1 shows a comparison of best efficiency points of low specific speed centrifugal pumps and Sta-Rite (commercial) regenerative pumps. Data from Ref. 3 and 4.

** Superscripts refer to references found in the Bibliography.

investigation. In each of the designs, the impeller has radial teeth or vanes machined at the periphery or cast on the face. The fluid passes through an open annular chamber, called the channel, and circulates repeatedly through the impeller vanes. It is from this internal "multi-staging" or "regeneration" that the pump properly derives its name. Closing the circuit between the inlet and outlet is the stripper or septum. In this region the open channel closes to within a few thousands of an inch of the sides and tip of the rotor allowing only the fluid within the impeller to pass through to the suction side of the pump.

2. CIRCULATORY FLOW THEORY

The expressions to be derived are based on a theory proposed by Wilson, Santalo, and Oelrich[5]. Due to changes in the geometry of the impeller and channel passages, the original expressions of Wilson, et al, cannot be applied directly. The same methods and reasoning are employed in the following section as were used in the original development of the theory.

2.1 Theory of Operation

2.1.1 The Fluid Mechanism

The flow within the pump is described as a helical motion by means of two perpendicular components of velocity at each point: the tangential component V_t and the component V_c in the plane perpendicular to V_t. The two terms introduced are:

(1) Tangential or through-flow: $Q = \int_A V_t dA$

where A is the cross-sectional area of the channel.

(2) Circulatory or meridional flow: Q_c with units of volume rate per radian arc length.

The angular momentum of the flow is increased as it passes radially through the impeller due to the guidance of the impeller vanes. In the channel the flow loses angular momentum and thereby supports a tangential pressure gradient in the channel. The flow then re-enters the impeller for another cycle. In order to increase the tangential pressure gradient, the rate of circulation must be increased and/or the tangential velocity of the flow entering the impeller must decrease. Reduction of the tangential velocity will cause a smaller through-flow.

The centrifugal field created by the impeller is constant if the rotor speed is constant, but the centrifugal field in the channel reduces as the through-flow is decreased. Consequently, as the channel centrifugal field is reduced, the driving force for the circulatory flow and the circulatory flow itself become greater. This accounts for the fact that both head and power are inversely proportional to through-flow as experimental results indicate.

2.1.2 Areas of Operation

Fig. 3 shows schematically the regenerative pump considered. Fig. 4 is an experimental curve of head variation of the fluid as it circulates through the pump for several flow rates. Three distinct areas of operation can be seen.

(1) Inlet and acceleration region. It is in this portion of the pump that the flow experiences a head loss through the inlet port and an acceleration from inlet velocity to the velocity of the existing flow pattern. This region is between inlet and taps 2 and 8.

(2) Linear region. In this section between taps 2 and 8 (227^{o}) the pressure gradient is essentially constant. This region is sometimes referred to as the working section of the pump for it is within this region that the useful head rise is developed.

(3) Deceleration and outlet region. Beyond the point of tap 8, the flow experiences a deceleration as well as turning in order to leave through the exit port. Due to deceleration there is a slight pressure rise followed by a throttling loss through the exit port.

A more detailed description of regions of operation can be found in References 1 and 5.

2.2 Derivation of Performance Expressions

2.2.1 Assumptions

To obtain working equations for the pump a theory of the fluid mechanism is developed involving a hypothetical model which represents only the linear section of operation and incorporates the following assumptions.

1. Flow may be considered steady if time averages are used for pressures and velocities.
2. Fluid is incompressible.
3. There is no internal leakage.
4. All processes within the pump are adiabatic.
5. Characteristic flow is one dimensional in each major direction (radial, tangential and axial).
6. Tangential pressure gradient is independent of radius.

The assumption of one dimensionality of the flow in each direction includes the assumption that the flow area leaving the impeller is equal to the flow area entering the impeller. There is no distinction in the actual pump between circulatory and tangential flow; they are only convenient components.

2.2.2 Control Volumes

A control volume of differential, $d\Theta$, of channel fluid is isolated and the steady flow energy equation and angular momentum relations are applied. A similarly shaped element of the impeller fluid is operated upon by the same relations. Appendix A-1 shows in detail this derivation.

Operation upon the channel element shown in Fig. 5 yields:

$$\frac{1}{\rho}\frac{dP}{d\theta} = \frac{Q_c}{R_2 A}\left[\sigma R_0 U_0 - \alpha R_i U_i\right] - gH_t \qquad (1)$$

by angular momentum considerations

$$\frac{P_o - P_i}{\rho} = \frac{\alpha^2 U_i^2 - \sigma U_0^2}{2} + \frac{Q}{R_2 A}\left[\sigma R_0 U_0 - \alpha R_i U_i\right] - gH_{cc} \qquad (2)$$

by the steady flow energy equation

$$\sigma = \frac{V_t \text{ actual}}{U_o}$$

$$\alpha = \frac{V_t \text{ actual}}{U_i}$$

where gH_{cc} = circulatory flow losses in the channel area

gH_t = tangential flow losses in the channel

Application of the same relations to the impeller element:

$$\frac{dW}{d\theta} = \rho Q_c \left[\sigma R_0 U_0 - \alpha R_i U_i\right]\omega \qquad (3)$$

by angular momentum considerations

$$\frac{P_o - P_i}{\rho} = \sigma U_0^2 - \alpha U_i^2 + \frac{\alpha^2 U_i^2 - \sigma^2 U_0^2}{2} - gH_{ci} \qquad (4)$$

by steady flow energy equation

where gH_{ci} = circulatory flow losses in the impeller passages.

Equations (2) & (4) are expressions for radial pressure rise between the same two points (via different paths), and hence, must be equal. By equating these two, a theoretical expression for circulatory flow head losses is obtained.

$$gH_c = gH_c + gH_c = \left(\sigma U_0^2 - \alpha U_i^2\right)\left(1 - \frac{Q}{R_c A \omega}\right) \tag{5}$$

2.3 Introduction of Loss Parameters

It is postulated that the circulatory flow experiences two resistances which cause losses in head. They are:

(1) Blade entrance loss. The flow in the channel about to enter the root of the impeller passage has a velocity much less than the blade. As it enters the passage, its tangential velocity is suddenly increased to the tangential velocity of the blade passage. This sudden acceleration or "shock loss" can be evaluated as a kinetic energy term. Spannhake[6] suggests:

$$\text{blade entrance loss} = \frac{(1-\alpha)^2 U_i^2}{2} \tag{6}$$

(2) Friction or turning losses. The fact that the circulatory flow is in contact with a surface at all times denotes that there is a wall shear stress. There are also turning and turbulence losses in the channel and blade passages. These losses are evaluated as proportional to the circulatory flow velocity squared.

$$\text{friction losses} = k_c \left(\frac{Q_c}{r_i b_i} \right)^2 \tag{7}$$

Accordingly, the resulting expression for circulatory flow losses is:

$$g H_c = \frac{(1-\alpha)^2 U_i^2}{2} + k_c \left(\frac{Q_c}{R_i A_i} \right)^2 \tag{8}$$

2.4 Performance Expressions

By equating the assumed head loss expression to the one derived from the theory, Eq. (5), an expression for the circulatory flow is obtained.

$$Q_c = \frac{R_i \theta_i}{\sqrt{k_c}} \sqrt{(\sigma U_0^2 - \alpha U_i^2)\left(1 - \frac{Q}{R_i A_w}\right) - \frac{(1-\alpha)^2 U_i^2}{2}} \tag{9}$$

There is still one parameter to be calculated theoretically. The through-flow, Q, is given by these two expressions:

$$Q = \int_A V_t \, dA \simeq \frac{\sigma U_0 + \alpha U_i}{2} A \tag{10}$$

The assumption of linear velocity gradient through the channel gives the simpler expression. In previous work on a different geometry this assumption was proved reasonable; it was employed on this analysis on that basis only.

The desired result is an expression for the head rise or pressure gradient in terms of the through-flow which can be evaluated and compared to experimental data. Eq. (1) shows the head rise to be proportional to the

circulatory flow and change of angular momentum. Eq. (9) evaluates Q_c ; substituting gives an expression for head rise as a function of σ , α , Q, and geometry.

$$\frac{1}{\rho}\frac{dP}{d\theta} = \frac{R_i B_i}{A}\sqrt{\frac{1}{k_c}}\left[\sigma R_0 U_0 - \alpha R_i U_i\right]\sqrt{\left(\sigma U_0^2 - \alpha U_i^2\right)\left(1-\frac{Q}{R_c A_w}\right) - \frac{(1-\alpha)^2 U_i^2}{2}} - g H_t \qquad (11)$$

Eq. (10) will give α as a function of σ & Q. This permits evaluation of the head rise as a function of through-flow only if σ & k_c are previously determined. Accordingly, by matching experimental values at two points, σ & k_c for the pump may be fixed and a match of theoretical and experimental curves may be obtained. In Appendix A-1 these expressions are non-dimensionalized for ease in handling.

3. DESIGN PROCEDURE

3.1 Loss Considerations

According to the theory there are two methods of improving the performance of the pump. That is to say, there are two major loss reductions which would increase performance (higher head at a particular flow). The losses which should be reduced are the blade entrance (shock) and circulatory friction losses (H_t & H_c).

The blade entrance losses will always be present when there is a difference in direction of the relative circulatory flow and the angle of the rotor blade passages where the flow re-enters. It would be possible to chamfer or tilt the blade passages at an angle of attack to reduce the kinetic energy loss to zero at a particular flow.

The circulatory flow friction losses are the result of turbulence and eddies set up by the corners and surface areas of the channel walls and blade passages. Several tests[1] were run on the inverted "L" shaped pump with one of the corners rounded, and improvement in head was noted.

At the time of design, improvement by tilted blades was thought to give only "localized" benefits with heavy sacrifices in performance at other operating points. In a later section, the effect of blade angles is theoretically predicted. It was felt absolute improvement would occur if all the corners in the channel and blade passages were rounded. This geometry of least circulatory resistance would be a torus as shown in Fig. 6.

Insertion of the filler torus was to observe what happens when the flow is induced to follow a helical pattern which is well defined. No

rationalization of losses was made to justify insertion of the fillers.

3.2 Theoretical Performance Predictions, "Friction, Factor, Theory"

The geometry of the new unit was unique and the data available on loss parameters could not be used in predicting performance. The similarity of the simple fluid coupling led to the "friction factor" theory derived in more detail in the Appendix.

The head losses are accounted for by these two expressions:

$$gH_c = \frac{(1-\alpha)^2 U_1^2}{2} + \frac{f}{2}\left(\frac{Q_c}{R_1 \theta_1}\right)(R_c \omega)$$

where f = 0.45 to 0.48 essentially constant for all flows. Wislicenius[3] employed this expression to predict performance of fluid couplings. However, the shock loss term is quite negligible as the reader can well imagine. The same values of f were used in the pump analysis despite the fact the fluid coupling has two rotors and the pump only one. This was looked upon as a margin of safety in the prediction.

The prediction of pressure coefficients based upon this assumed loss expression were 4 to 5 times greater than actual data. The mistake was, as the Appendix points out in more detail, in the friction loss expression. Despite the physical similarity between the new unit and the fluid coupling, the actual flow mechanisms are not completely similar.

3.3 Experimental Unit

The new unit bears a geometrical relationship to the lucite model of Santalo[1]. The ratio of channel area to peripheral rotor diameter squared is

constant. An outside diameter of 9.5" was selected, the required channel area was 1.54 in^2 which was a 2" dia torus shaped channel. The radius ratios, r_i/r_o, of Santalo's configurations ranged from 0.72 to 0.89 while the ratios encountered in this investigation were from 0.64 to 0.72.

The filler torus used in the investigation were 3/4" and 1 1/4" dia. The outside diameters of the rings are such that the areas of circulatory flow entering and leaving the blade passages are equal.

4. DESCRIPTION OF APPARATUS AND TEST PROCEDURE

4.1 Description of the Pump Unit

Details of the unit constructed are shown in Fig. 6 and again in the photographs in the Appendix. The essential elements include:

1. Impeller with 40 radial teeth cast from a low melting alloy. D = 7.50".
2. Casing of machinable steel with a half-torus channel, 2" dia.
3. Support plate for casing, serving also as a back cover.
4. Four radial seals with a running clearance of 0.008".
5. Axial inlet and outlet ports (cast of plaster of Paris).
6. Stripper or septum region (cast of plaster of Paris).
7. Clearance between impeller face and casing about 0.005".
8. Filler rings or torus - 3/4" and 1 1/4" dia.

The outside diameters of the fillers were determined by requiring equal areas of flow in and out of the impeller face. Geometrically, this means $r_i b_i = r_o b_o$.

Special efforts were made during the design of the unit to allow for future alterations. The stripper region and ports are cast of plaster of Paris using a clay mold. The teeth are cast from a low melting alloy to permit easy remelting and casting should a new blade shape or geometry be desired.

4.2 Instrumentation

The instrumentation installed on the unit included:

1. Venturi tube with inclined manometer at inlet.
2. Static pressure taps connected to a water manometer. Tap locations are shown in Figs. 3 & 6.
3. Cradled dynamometer (electric) rated at 2.62 in.-lb. torque. Sliding weight on a calibrated arm measured the torque.
4. Commercial strobatac to measure speed of rotation.

4.3 Apparatus

Tests using air as the pumping fluid were run on three pump configurations - no filler, 3/4" filler, and 1 1/4" filler. Constant speed tests at 950, 1000, 1150, and 1250rpm (2 speeds per configuration)* were used to correlate data on a dimensionless basis. In order to cover the full range of the pump (internal performance), it was necessary to "help" the fluid overcome the inlet and outlet port resistances by use of a vacuum cleaner attachment. During the entire investigation, no changes in stripper (except to accommodate the filler) or radial clearances were made in an effort to eliminate the effects of leakage upon performance.

4.3.2 Instrumentation

The following procedure was used in obtaining experimental data:

(1) Through-flow was measured by a venturi meter and varied by a control (gate) valve. At shut-off (control valve closed) there was a

---

* Critical speeds of the impellers and dynamometer power limitations played a role in the selection of these speeds.

net through-flow. This leakage was attributed to the radial seals and an appropriate correction to measured through-flow was necessary. This correction procedure is explained in the Appendix.

(2) Pressure variations in the linear section were measured by water manometers. The point of zero head rise was obtained by manipulating the control valve until the pressure levels at taps 2 and 8 were equal. This operation involved use of the vacuum cleaner attachment.

(3) Torque measurement was by a dynamometer with calibrated arm and sliding weight. Difficulty was experienced in obtaining a constant "static" tare weight of the unit due to the large moment of inertia of the impeller. The tare reading was taken as the reading at zero pressure coefficient, automatically assuming power was zero at this point. Except for frictional and drag forces, this is a reasonable assumption. However, this reading was within the range of oscillation of the "static" tare readings and was assumed as the "true" tare weight.

(4) Speed measurements were obtained by a commercial strobotac. A Variac was used to control the speed.

5. DISCUSSION OF EXPERIMENTAL RESULTS AND ANALYSIS

5.1 Performance Curves, Fig. 7

5.1.1 Similitude Conditions

The regenerative pump has been shown to be a hydrodynamic unit obeying all the laws of similitude which govern axial-flow and centrifugal machines[1, 8]. In order to show similitude conditions existed for the new pump, results of the tests were correlated on a dimensionless basis.

The dimensionless parameters involved are:

flow coefficient $$\varphi = \frac{Q}{R_c A \omega} = \frac{Q}{Q_s}$$

head coefficient $$\frac{d\Psi}{d\theta} = \frac{g H}{\omega^2 D^2} \cdot \frac{1}{\theta_p}$$

power coefficient $$\frac{dP}{d\theta} = \frac{g \tau}{\rho \omega^2 D^5} \cdot \frac{1}{\theta_p}$$

efficiency $$\eta = \frac{\rho Q H}{W} \quad \frac{\frac{d\Psi}{d\theta} \cdot \varphi}{\frac{dP}{d\theta}} \cdot \frac{R_c A}{D^3}$$

The flow coefficient is the ratio of corrected measured through-flow to solid body rotation of the channel area at wheel speed. The power and head coefficients and efficiency are the more familiar expressions common to many turbo-machines.

5.1.2 Improvement in Performance

Santalo[1] reported a $\frac{d\Psi}{d\Theta} = 0.25$ for the best inverted "L" channel type pump as compared to $\frac{d\Psi}{d\Theta} = 0.40$ for the new unit. Santalo's pressure coefficient was based upon the velocity head at the periphery of the wheel, while the author's is based upon an average velocity head at the centerline of the channel area. Also, one must keep in mind, geometry effects are present. Despite the differences, the net result seems to be that the effectiveness of the new unit in producing higher heads has been increased.

In the practical operating region of the pump $\varphi = 0\text{-}0.5$, the internal (and sometimes external, too) efficiency is very nearly equal to the theoretical limit of Q/Q_s [2] for all types of regenerative pumps. Improvement in this range could not be significant.

Of greater interest is the magnitude and φ value of the maximum efficiency point. It is the author's, and his colleagues, impression that $\eta_{max} = 0.64$ @ $\varphi = 0.8$ is an improvement over previous units. Unfortunately, there is no data available on internal efficiencies so no direct comparisons can be made.

5.2 Theoretical and Experimental Head Curves, Fig. 8

5.2.1 Method of Obtaining Theoretical Constants

According to the postulated theory, there are two constants which determine the theoretical performance of the pump. They are the slip factor and the circulatory flow friction factor. In order to

evaluate these two constants, the dimensionless expression for the head rise as derived in the Appendix is employed.

$$\frac{d\psi}{d\theta} = \frac{R_i B_i}{A}\sqrt{\frac{1}{2k_c}}\sqrt{\frac{R_c}{R_i}}\,(C_1-\psi)\sqrt{(C_1-\psi)(1-\psi)-\frac{R_c}{R_i}(C_2-\psi)^2} \quad *$$

The following method was employed in obtaining values of k_c and τ.

(1) At $\frac{d\psi}{d\theta} = 0$ and ψ_{max} either $(c_1-\psi)$ or the expression under radical must be zero. The radical represents the circulatory flow which is theoretically zero at $\frac{d\psi}{d\theta} = 0$.

(2) Substitute $\psi = \psi_{max}$ in the radical and equate to zero, the result will yield a value of τ.

(3) The shape of the $\frac{d\psi}{d\theta}$ curve is now determined but the absolute values are unknown until k_c is evaluated. At a particular ψ, $\frac{d\psi}{d\theta}$ has an experimental value. By matching the theoretical and experimental curves at this point, a value of k_c may be obtained and a match of theoretical and experimental curves should result.

---

* c_1 & c_2 are derived in the Appendix

$$C_1 = \frac{R_o^2}{2R_i R_c}\left(1+\frac{R_i}{R_o}\right)\tau \qquad C_2 = \frac{R_i^2}{2R_c}\left(1+\frac{R_o}{R_i}\tau\right)$$

Table I (Appendix) shows the values involved in matching the experimental head curves for the three configurations tested. The match point for determining k_c was $\phi = .3$ in each case. The points for determining Ψ values are recorded in the Table.

5.2.2 Adjustment of Characteristic Streamline Radii

Previous investigators used values at two points in solving two simultaneous equations for arriving at values of Ψ & k_c. Even though a match was forced at two points, there was no guarantee the curves would coincide at other points. To insure a good fit, it was necessary to adjust the values of r_o and r_i. This was an arduous procedure but produced a curve of the proper "shape".

The values of r_o and r_i are the radii at which the average streamline leaves and enters the impeller. In an "inverted L" channel or in an open torus channel it is not obvious what values r_o and r_i should have. The author was forced to adjust these radii in the case of "no filler" to force a fit of experimental and theoretical curves, and the result was still a poor match, Fig. 8.

5.2.3 Effect of Fillers

The effect of inserting the fillers was to eliminate an adjustment of radii. The area of entry and exit to the impeller passages was small enough that there was little doubt that the characteristic streamline would pass near the centroid of the area. It was these geometric

values of r_o and r_i that were used in obtaining a fit for the filler pumps without any adjustment.

Fig. 8 shows this comparison of theory and data for the two fillers inserted. It is quite gratifying to the authors of the circulatory flow theory that the match is so good. Several other investigators have claimed that the matching of theoretical and experimental curves was "mathematical coincidence" caused by adjusting 3 constants - the radius ratio, σ and k_c values. The fact that no radii adjustments were made, and a good fit was obtained, shows the theory does represent the proper fluid mechanism.

5.3 Theoretical Constants

5.3.1 Slip Factor, σ

The slip factor σ is a measure of degree of guidance which the blade offers to the flow leaving the impeller. Fig. 10 shows this variation of σ as a function of filler diameter. This curve assumes that σ will be unity when the filler completely replaces the entire channel area or when the number of blades is infinite. One of the effects of the fillers was to restrict the flow causing it to leave and enter at certain areas. With no filler, the flow may leave the impeller over a large area and the size of the area may change with flow conditions. For this case, the degree of guidance would be less than with the filler, hence a lower σ value. The larger the filler, the better the guidance and consequently, the greater will be the σ value.

Bussman's data on η values (centrifugal pumps) as a function of radius ratios and number of blades does not compare with the experimentally determined radius. Bussman would predict $\eta = 0.95$ for all the configurations[1]. This deviation is explained by the different nature of flow leaving the regenerative pump as compared to the centrifugal pump.

5.3.2 Circulatory Resistance Factor, k_c

The meaning of the variation in k_c is difficult to interpret for its value depends upon several parameters including r_o, r_i and φ. A look at k_c in terms of skin friction alone gives a simple explanation for a variation with geometry. Certainly rough channel walls will increase the resistance to circulatory flow (and also through-flow) and the only parameter that would account for this increased resistance would be the magnitude of k_c. In a similar manner, k_c would reflect an increase in area over which the circulatory flow travels, which in this case would be the filler. (Fig. 9 shows this variation.)

Fig. 11 shows k_c plotted as a function of L/D where: L is the average circumferencial distance of the filler and channel, and D_L is the hydraulic diameter. The dotted line is an average curve with the equation:

$$k_c = K_1 + K_2 \cdot \frac{L}{D_H}$$

where K_1 = constant

K_2 = a friction factor

The fact that k_c is not zero at $L/D_H = 0$ may be explained in part by saying k_c represents not just friction as described, but also includes effects of turning and turbulence. However, this expression shows that k_c is a function of geometry, but not a unique one.

5.4 Circulatory Flow Curves, Fig. 12

The entire fluid mechanism of the pump can be explained in terms of events which the circulatory flow experiences. The results of using the fillers in the pump have led to confirmation of the theory as well as added to the understanding of the actual mechanism.

Fig. 12 shows plots of $\frac{Q_c}{Q_s}$ obtained from experimental and theoretical expressions, (k_c and φ are experimentally determined). As one might expect, as resistance to circulatory flow is increased, the flow will reduce. This is shown by the magnitudes of the k_c values. The shape of the Q_c/Q_s curves can be explained by rationalizing what happens in the force field of the channel. Consider the channel as a curved tube and due to the curvature there will be a radial pressure gradient. At φ_{max} the gradient in the channel is large enough to offset the gradient produced by the impeller, hence, there is no circulatory flow. As φ is reduced, there is a pressure differential causing fluid to flow. The channel force field is decreasing as decreases and the driving force is the constant impeller field less all the losses. The circulatory flow will continue to increase as φ is reduced until it reaches a maximum point. At values of φ less than this, the shock losses begin to show their effect. The reader will remember the expression for the

shock losses which is proportional to a quadratic in ϕ with larger values at low ϕ's reducing to zero near $\phi \approx 0.9$ and then increasing slightly again as ϕ increases. It is these shock losses that reduce the available driving force for the circulatory flow.

The fact that there is less curvature in the configurations with the fillers can be attributed to the magnitude of the resistance losses in comparison to the shock losses. The shock losses in each configuration are approximately equal since r_o and r_i do not change appreciably. The resistance to circulatory flow changes in the configurations. The decrease in curvature of the Q_c/Q_s curves is due to the ratio of shock losses to resistance losses which decreases as k_c increases.

The deviations of theoretical from experimental Q_c/Q_s values have the same pattern as were seen in Fig. 8 in head curve comparisons. The "errors" in the theoretical expressions are greatest near shut off and are asymmetrical in a sense - above experimental values to the left of $\phi \approx 0.3$ and below to the right, or vice versa. The curves could be made to coincide by adjustment of radii. However, any variation of radii from the "centroid" value must be rationalized in terms of other flow parameters.

6. THEORETICAL PREDICTIONS ON "CHAMFERED BLADE" UNIT

6.1 Analysis of Basic Model

From the experimental results it is possible to predict, with some degree of confidence, the performance of a unit with chamfered blades. Specifically, the following analysis considers the 3/4" filler configuration with a blade angle β at the passage roots only.

Fig. 13 shows the velocity triangles used in computing the shock loss. It was assumed in this analysis that k_c and σ remain constant. The head loss assumption:

$$g H_c = \frac{\left[(1-\alpha) R_i \omega - \frac{Q_c}{R_i B_i} \tan\beta\right]^2}{2} + k_c \left(\frac{Q_c}{R_i B_i}\right)^2$$

was equated to the theoretical expression Eq. (5) yielding a quadratic in Q_c/Q_s.

$$\frac{Q_c}{Q_s} = + \frac{a}{2} + \sqrt{\frac{a^2}{4} + \varphi_c^2 \frac{1}{\tan^2\beta/2k_c + 1}}$$

where

$$a = \frac{2 \tan\beta (C_2 - \varphi)}{k_c \frac{A}{R_i B_i} \left(\tan^2\beta/2k_c + 1\right)}$$

$\varphi_c = \frac{Q_c}{Q_s}$ value for straight bladed impeller.

Figs. 14 & 15 show the effect of various angles of attack on the head curves and shock loss values.

6.2 Discussion of Theoretical Curves, Figs. 14 & 15

Fig. 14 shows the improvement in performance by chamfering the blades at the impeller inlet passages. The assumption of a constant σ value

is reasonable, but variations in k_c seem inevitable. The circulatory flow must pass through a curved passage instead of the straight radial one in the $\beta = 0$ impeller. Hence, the performance may be overestimated.

There is some doubt concerning the evaluation of the shock losses in the curved blade configurations. The method employed was suggested by Spannhake, but other experts suggest alternative methods. The shock losses no longer involve only decelerating flow (when $\beta = 0$) but also accelerating flow ($\beta > 0$). One might feel intuitively that accelerating turning losses would be less severe than decelerating ones - this would lead to over-evaluation of the shock losses for $\beta > 0$. Hence, the performance curves may be conservative.

Fig. 15 shows the comparison of shock losses for values of β. It would appear that $\beta = 60^{\circ}$ is nearly the optimum angle of attack, for the shock losses are very small throughout the entire range of operation.

7. CONCLUSION & RECOMMENDATIONS

7.1 Performance of the Experimental Unit

The experimental unit is an improvement over previously tested units in two respects. First, the maximum efficiency is greater and the point, ϕ, at which it occurs is larger. Second, the head coefficient at shut-off is greater than existing reported data. The increased performance must be attributed to lower resistance to circulatory flow. However, with pumps of different geometries comparison of all the parameters is not simple and must be interpreted critically.

7.2 Verification of the Existing Theory

7.2.1 Circulatory Flow

The use of the fillers to induce helical flow and define exit and entering flow area in the impeller passages was successful. The theoretical and experimental head curves were very favorably matched without adjustment of radii as previously required.

The values of Ψ & k_c obtained from the three pump geometries have shed light on the nature of the circulatory flow. Increased size of the filler causes greater resistance to flow and better blade guidance. Consequently, k_c and Ψ increase. The fact that there is less curvature in the head and circulatory flow curves as the fillers increased is explained by the decrease in ratio of shock losses to resistance losses.

7.2.2 Shear Stress Theory

There are several theories present in the literature today based upon the driving mechanism being a shear stress. The head rise is caused by the rapidly moving impeller sweeping past the slow moving channel fluid. The head curves of Fig. 8 can be produced as evidence to refute this theory. This theory says head rise is proportional to area of the impeller shearing the fluid. Consider the "no filler" and "1 1/4 filler" configurations. The "1 1/4" filler" effective blade area is reduced to 38% from the "no filler" value while the head is reduced to only 69%. The shear stress theory cannot account for the effects caused by a filler.

7.3 Recommendations

There is still much work that can be done in the way of improvement on performance. So far only the internal performance has been investigated. Improvement of inlet and outlet ports must be accomplished before over-all performance can be increased. The possibility of types of entry is large including combinations of tangential, axial, or radial entry and exit.

The design of the pump for this investigation centered around reducing one of two major losses within the pump. It has been shown that the torus channel has better performance due to lower circulatory flow resistance. Calculations based upon experimental data show that genuine improvement is possible with chamfered blades. An experimental program to demonstrate this would be quite useful.

EFFICIENCY COMPARISON

FIGURE 1

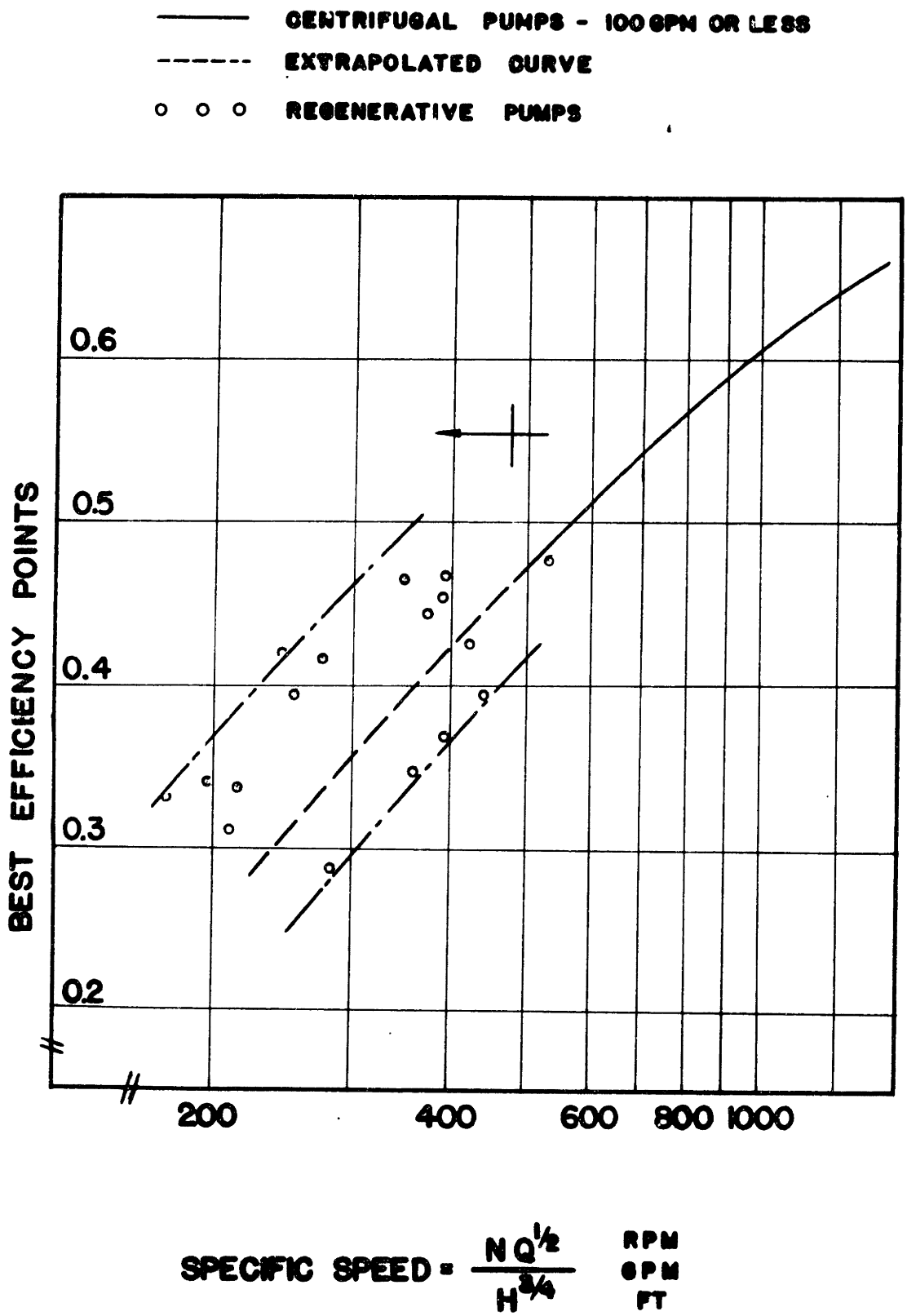

TYPICAL PUMP CROSS-SECTIONS

FIGURE 2

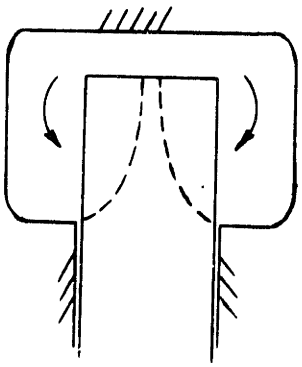

A. COMMERCIAL UNIT

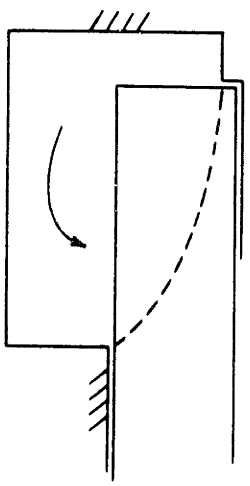

B. TEST UNIT

"INVERTED L CHANNEL"

C. TEST UNIT

"HALF TORUS CHANNEL"

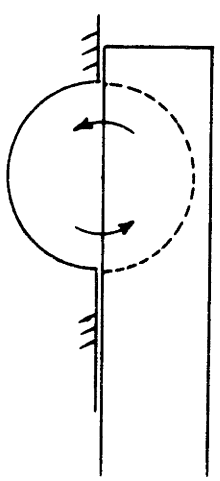

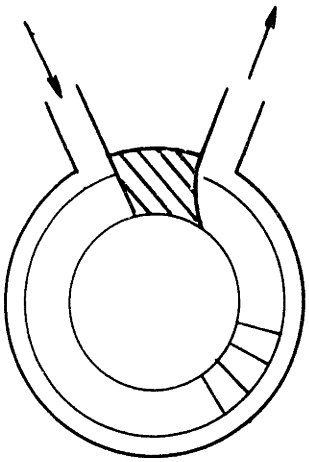

FRONT VIEW OF

UNIT B.

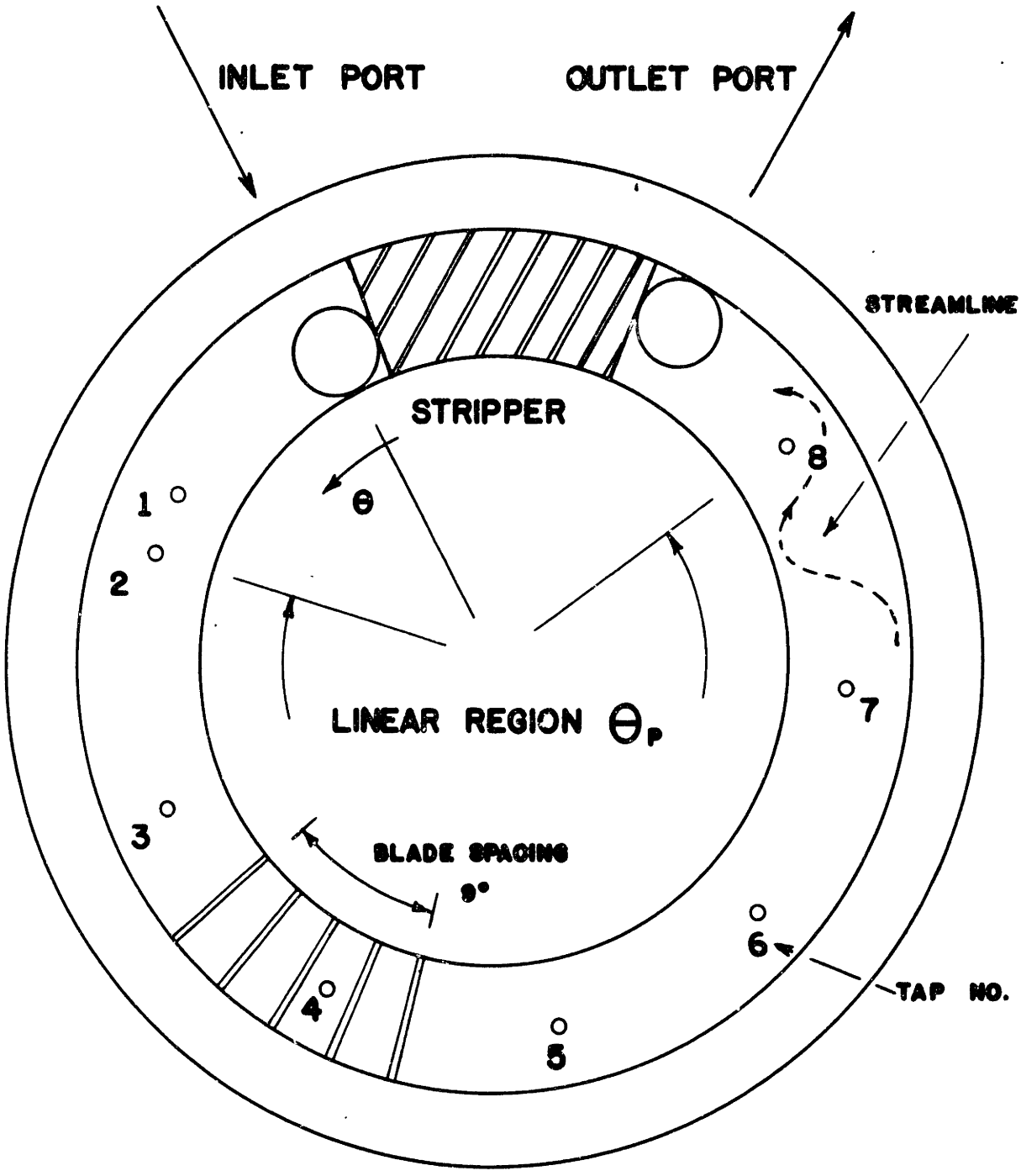

SCHEMATIC VIEW OF TEST UNIT

FIGURE 3

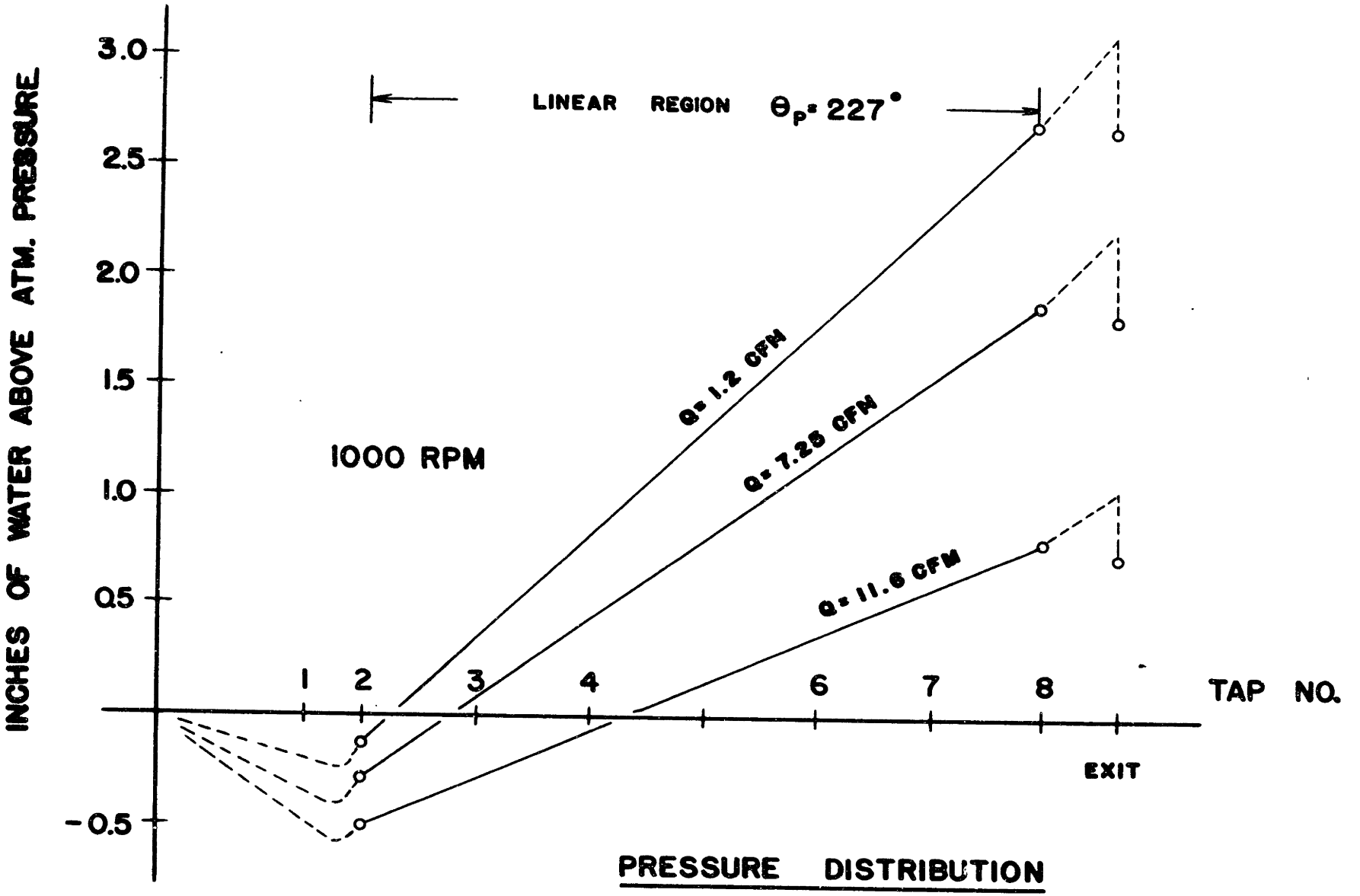

PRESSURE DISTRIBUTION

FIGURE 4

BASIC CONTROL VOLUMES

FIGURE 5

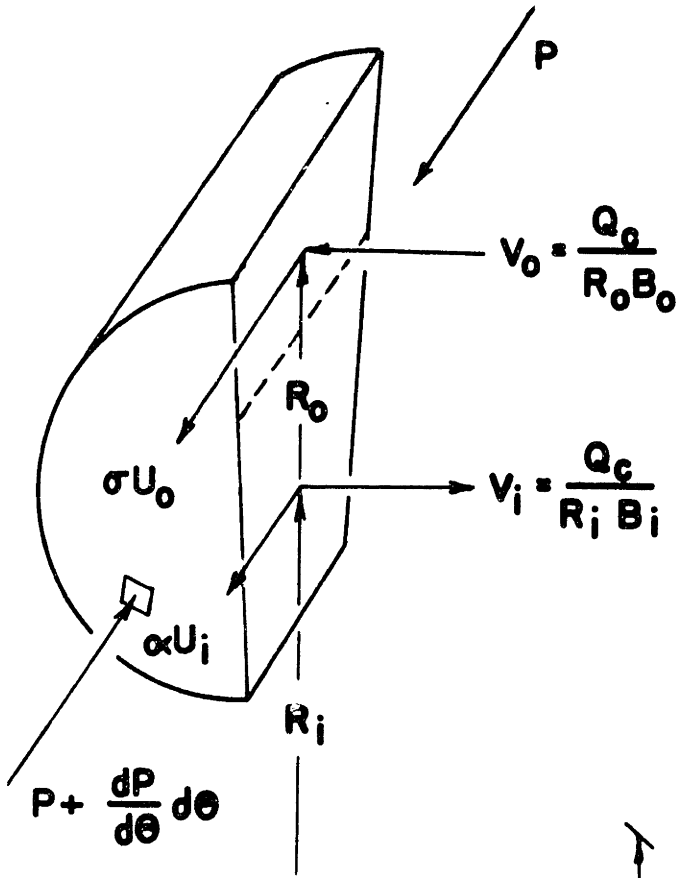

CHANNEL ELEMENT

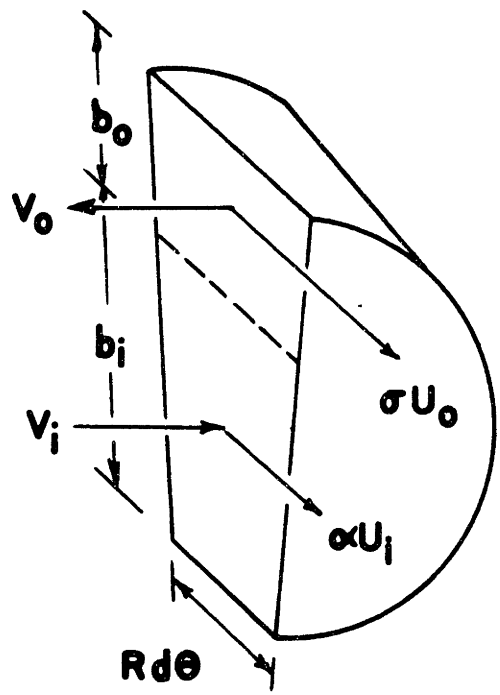

IMPELLER ELEMENT

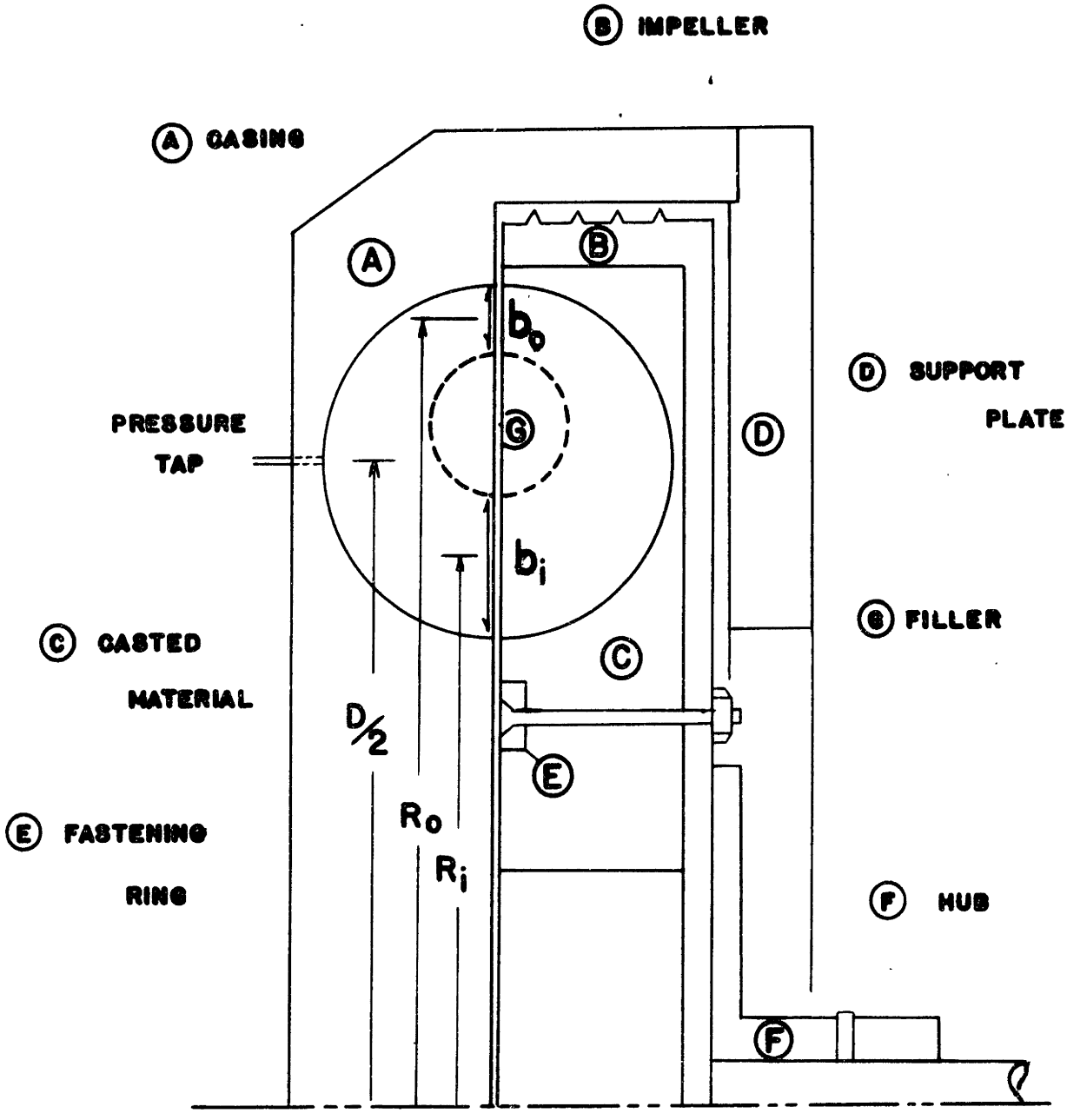

CROSS-SECTION OF EXPERIMENTAL UNIT

FIGURE 6

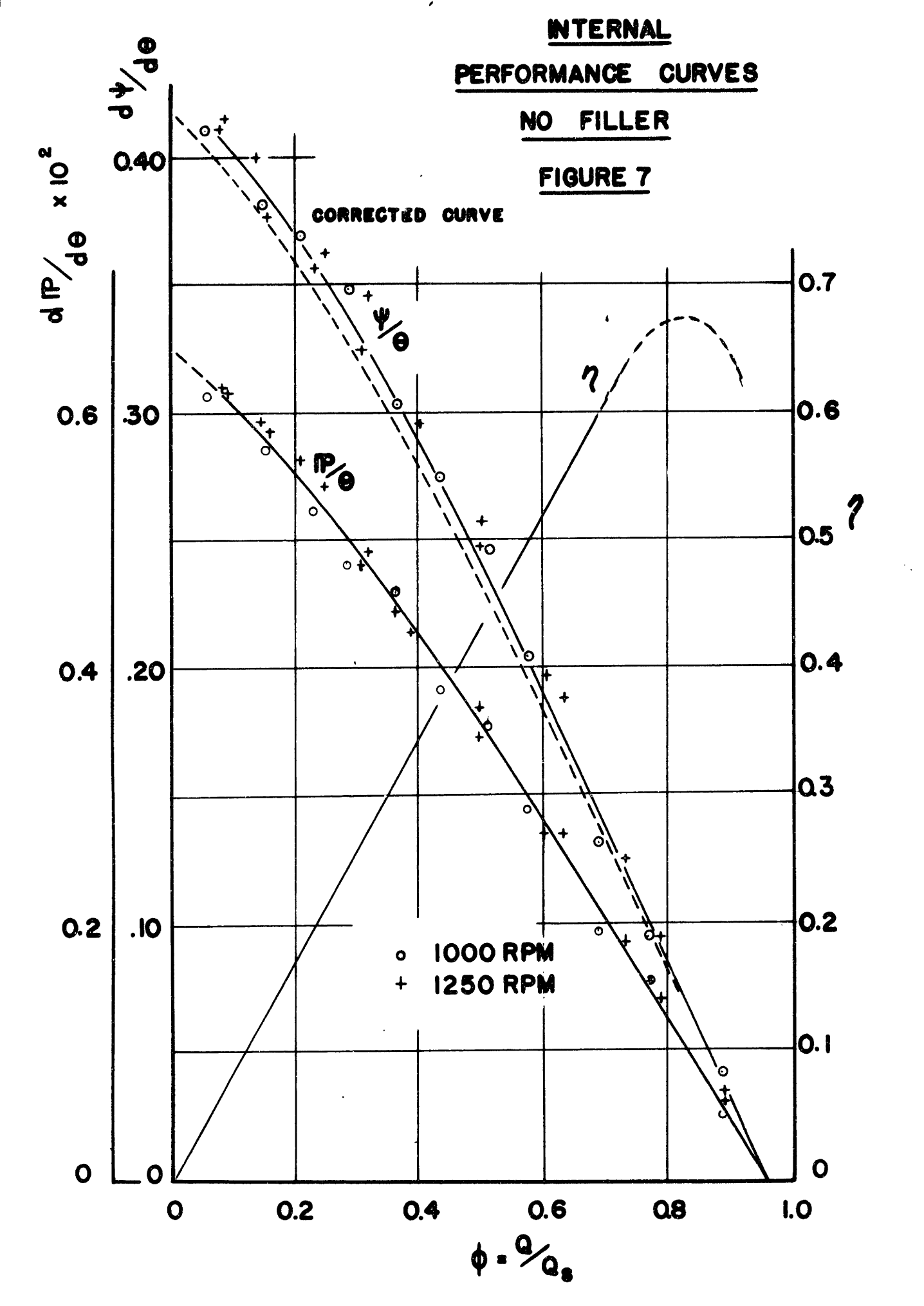
INTERNAL
PERFORMANCE CURVES
NO FILLER
FIGURE 7
CORRECTED CURVE
dΨ/dθ
dΠP/dθ x 10²
Ψ/θ
ΠP/θ
η
1000 RPM
1250 RPM
0.40
0.30
0.20
0.10
0
0.6
0.4
0.2
0.7
0.6
0.5
0.4
0.3
0.2
0.1
0
0.2
0.4
0.6
0.8
1.0
φ = Q/Qs

COMPARISON OF THEORETICAL AND EXPERIMENTAL HEAD CURVES

FIGURE 8

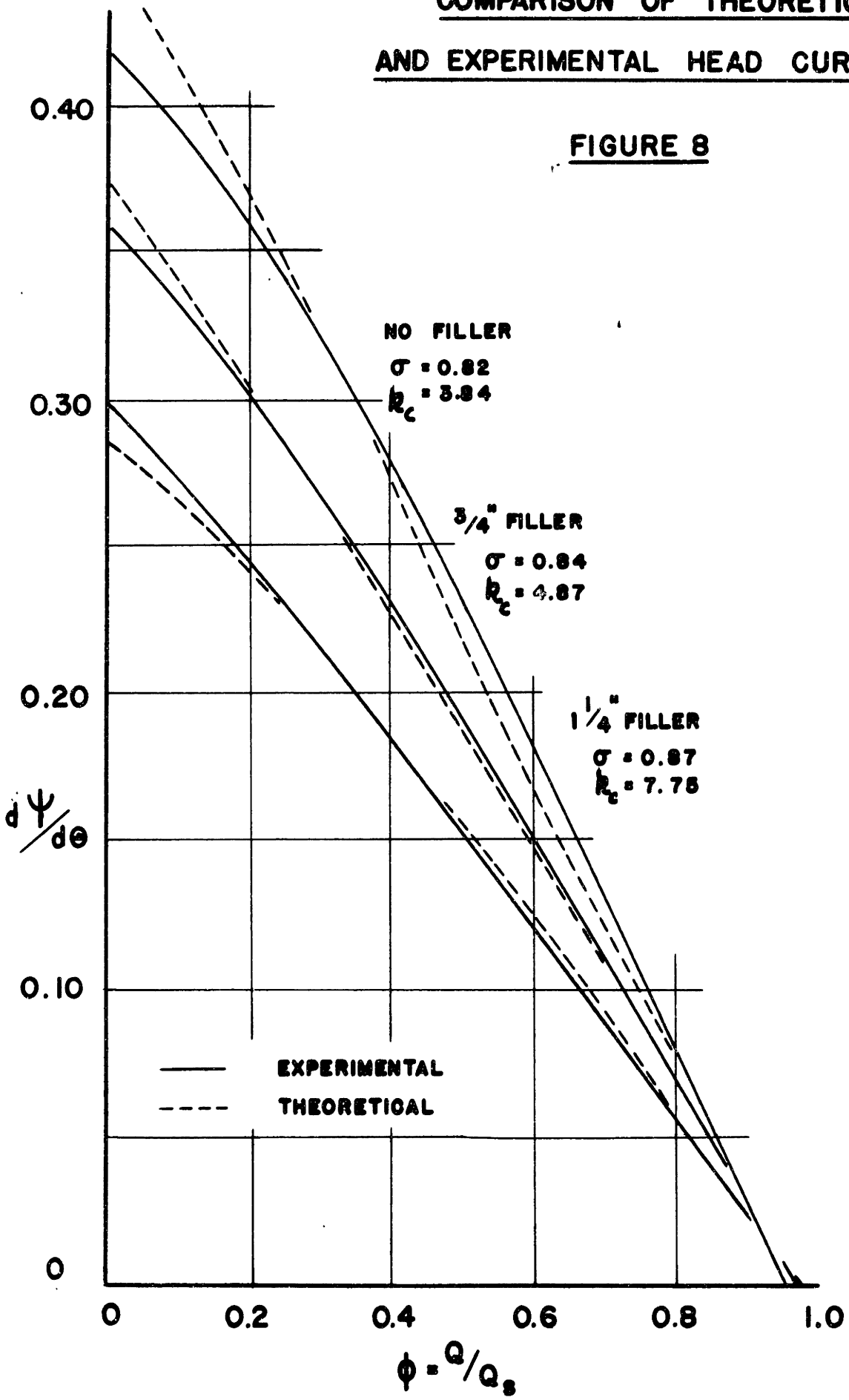

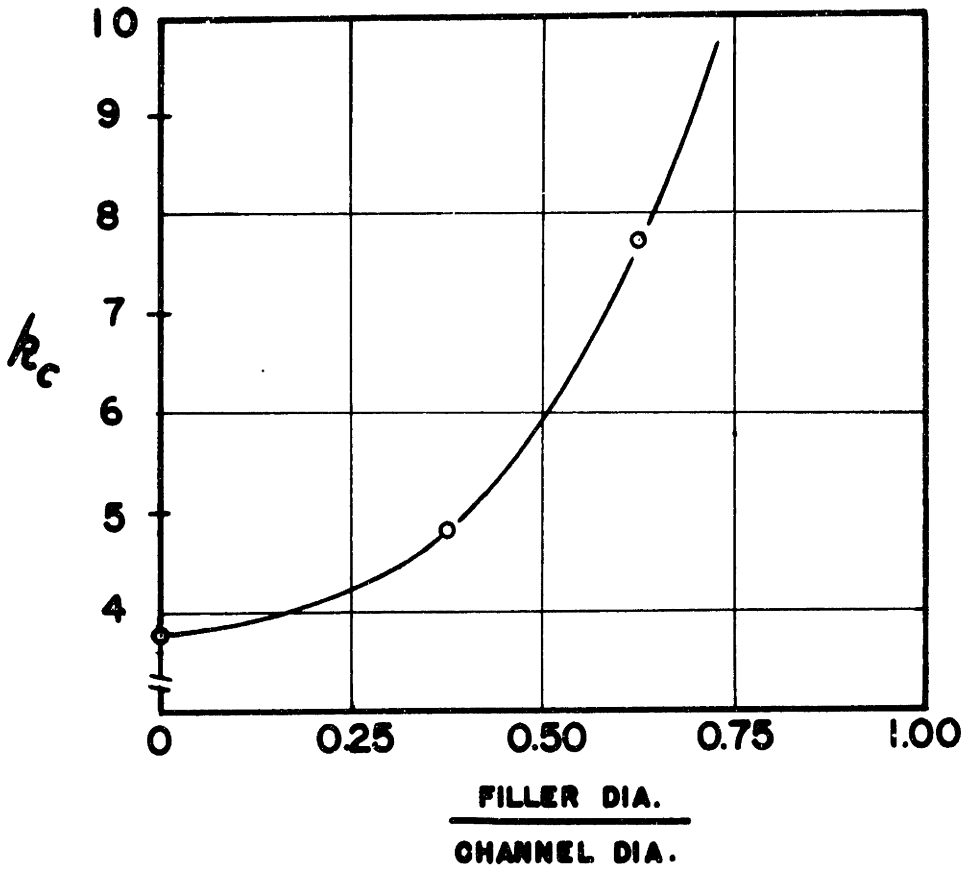

FIGURE 9

VARIATIONS OF σ AND k_c

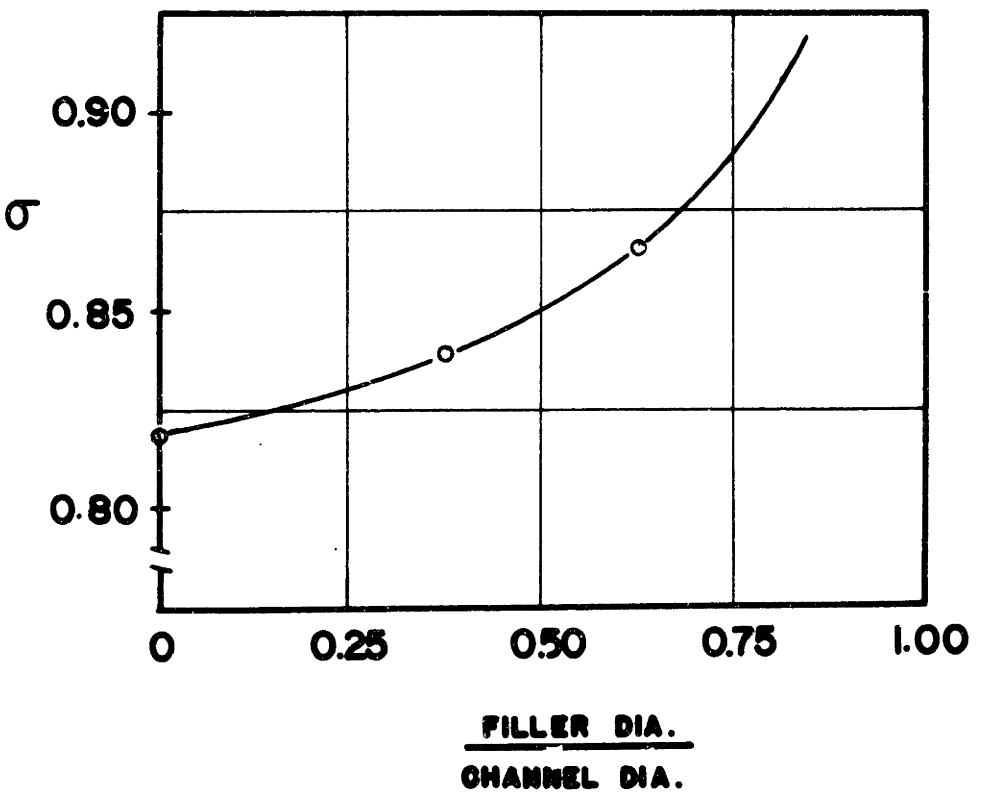

FIGURE 10

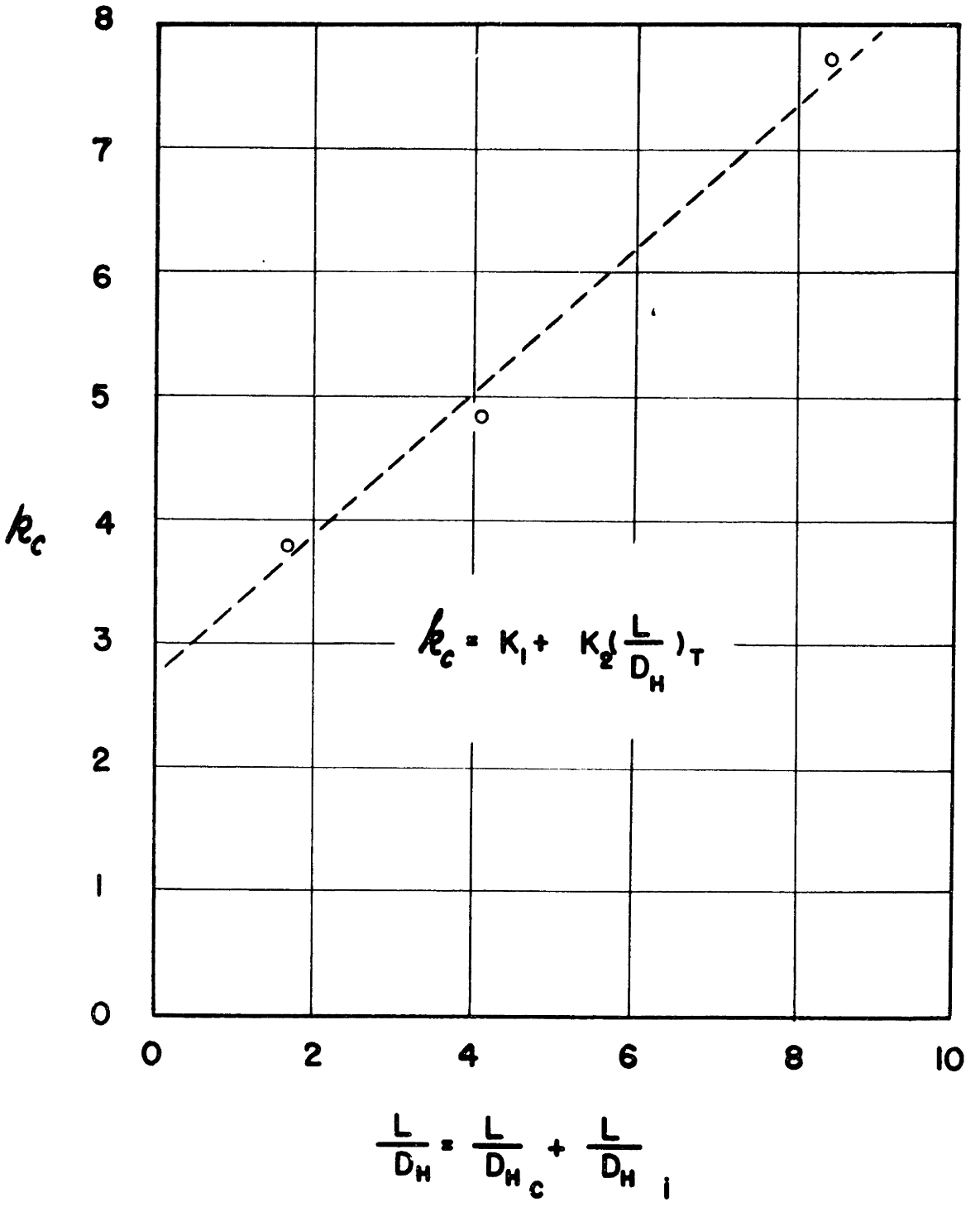

VARIATION OF k_c WITH $\frac{L}{D_H}$

FIGURE II

VARIATION OF CIRCULATORY FLOW

FIGURE 12

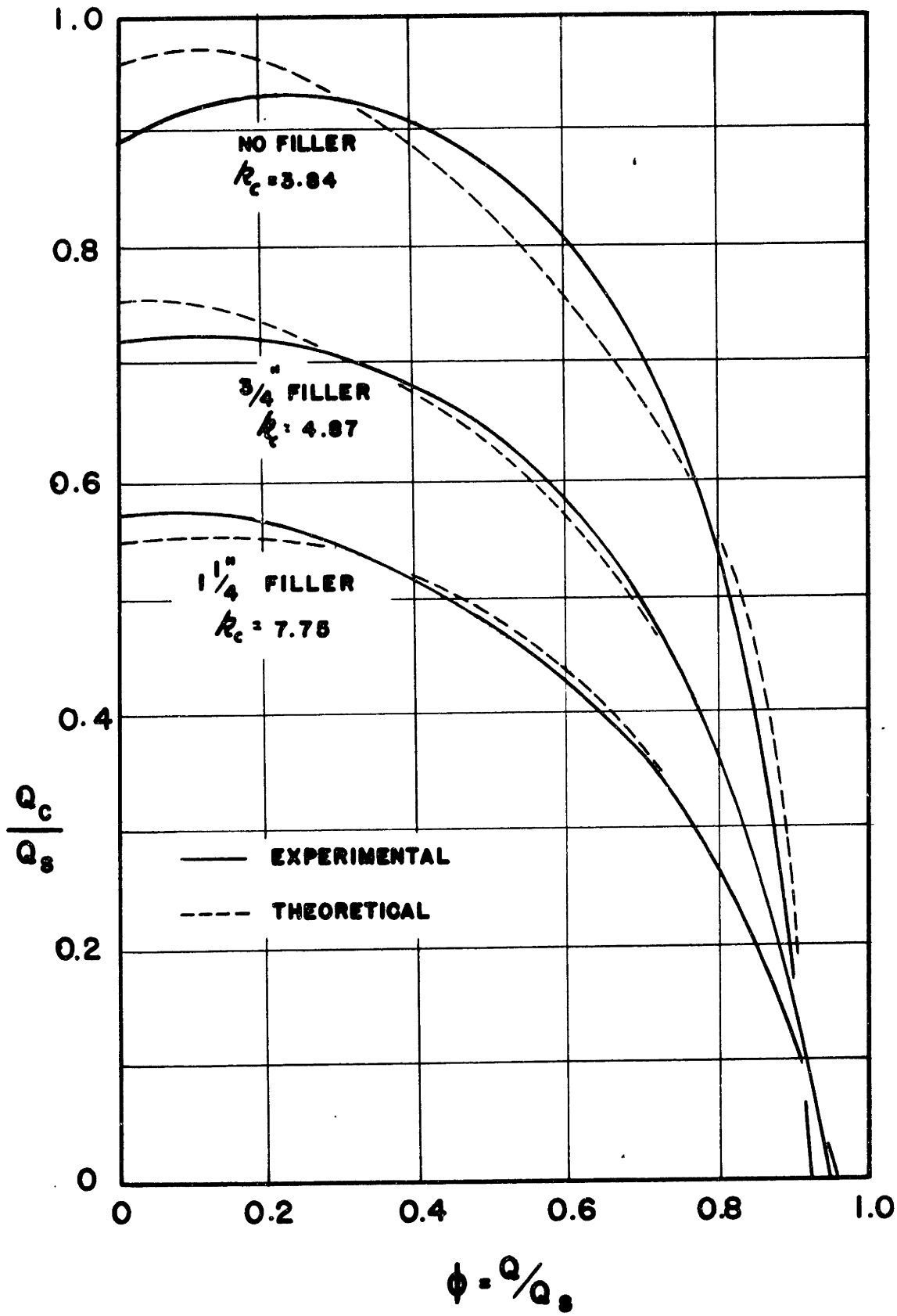

VELOCITY TRIANGLES

FIGURE 13

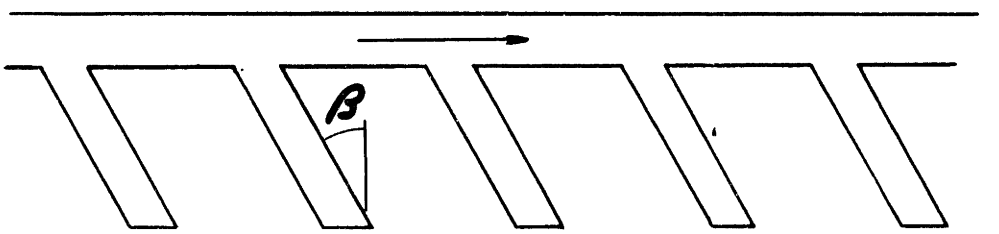

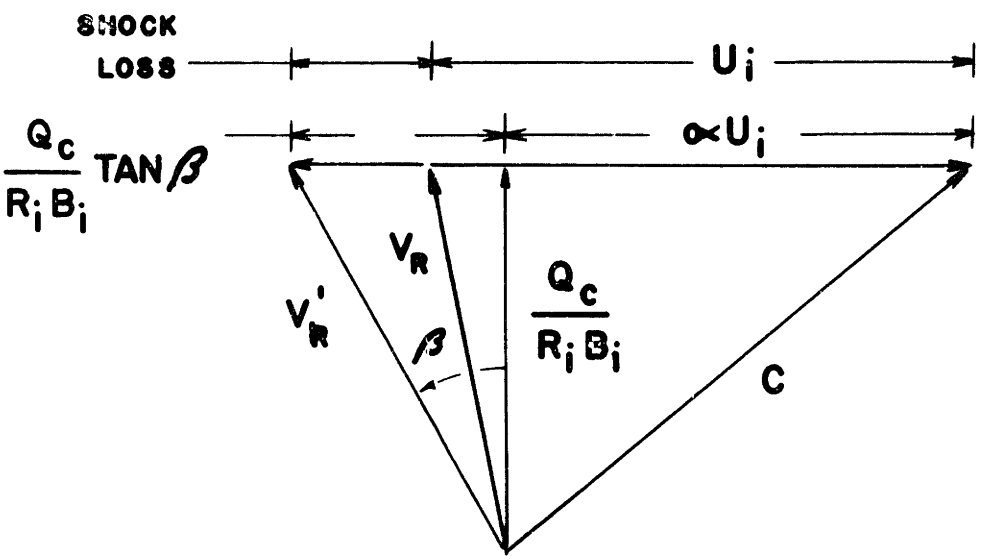

C - ABSOLUTE VELOCITY

V_R - RELATIVE VELOCITY

V_R' - VELOCITY IN DIRECTION

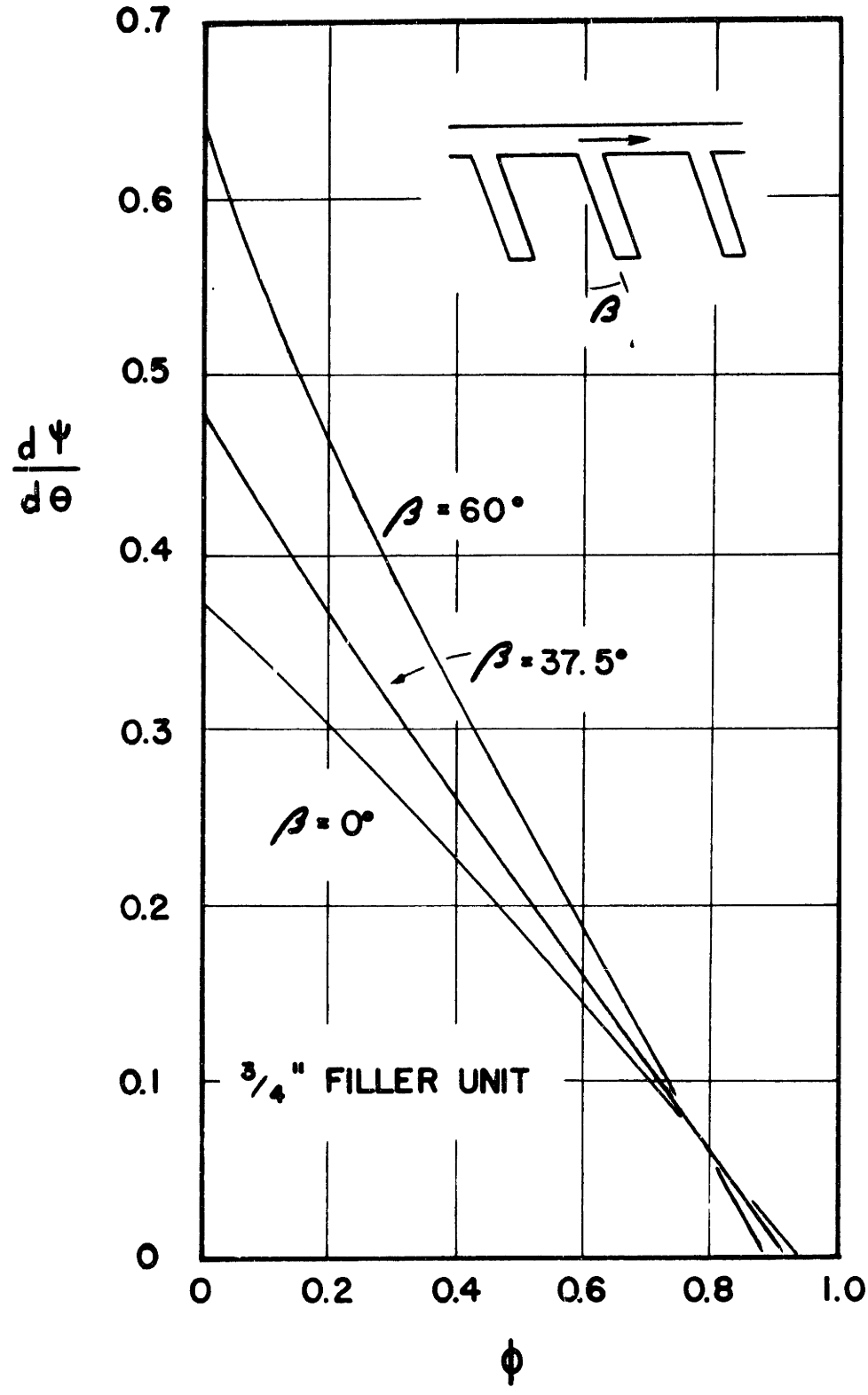

EFFECT OF BLADE ANGLE ON PERFORMANCE

FIGURE 14

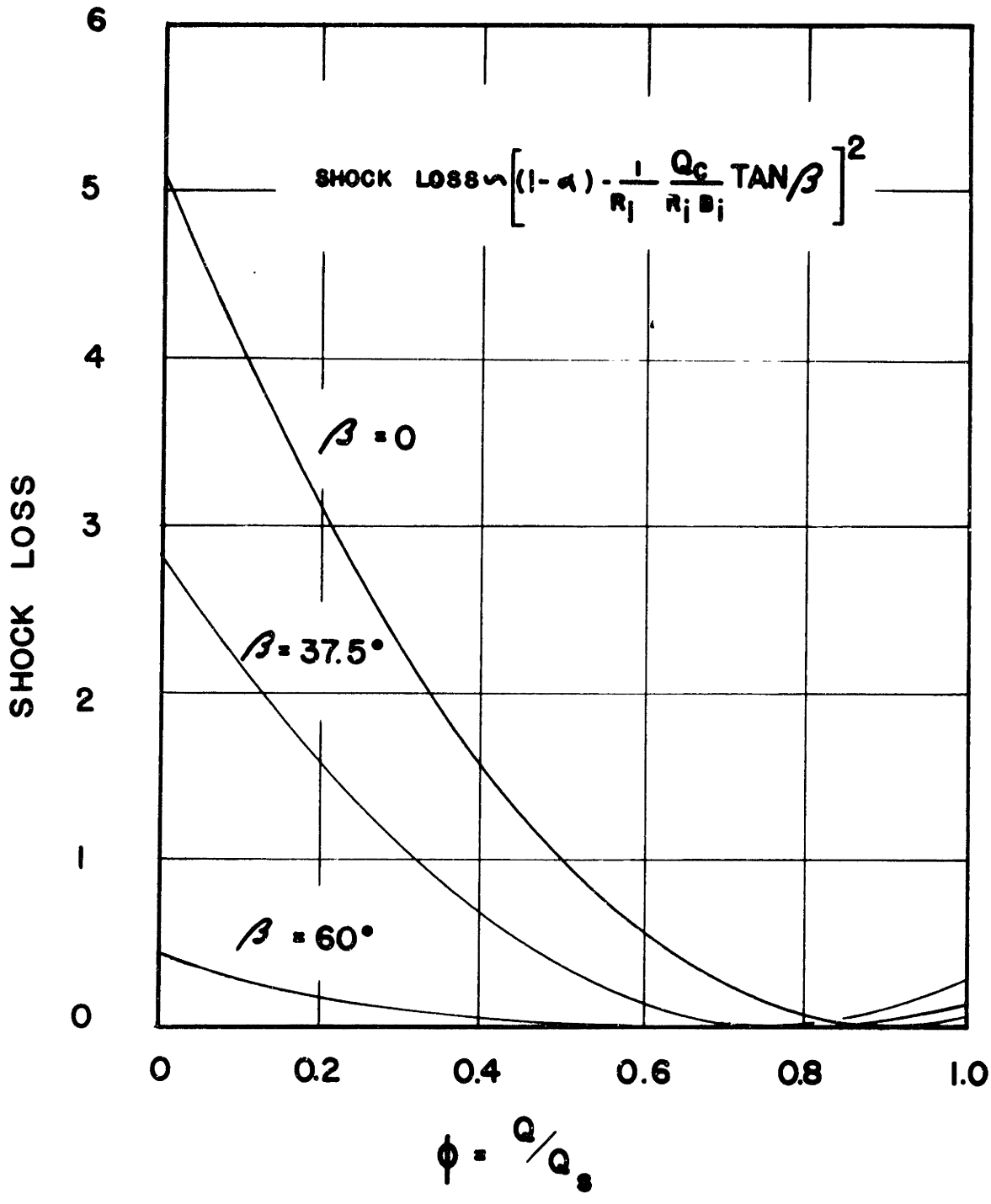

SHOCK LOSS VARIATIONS.

FIGURE 15

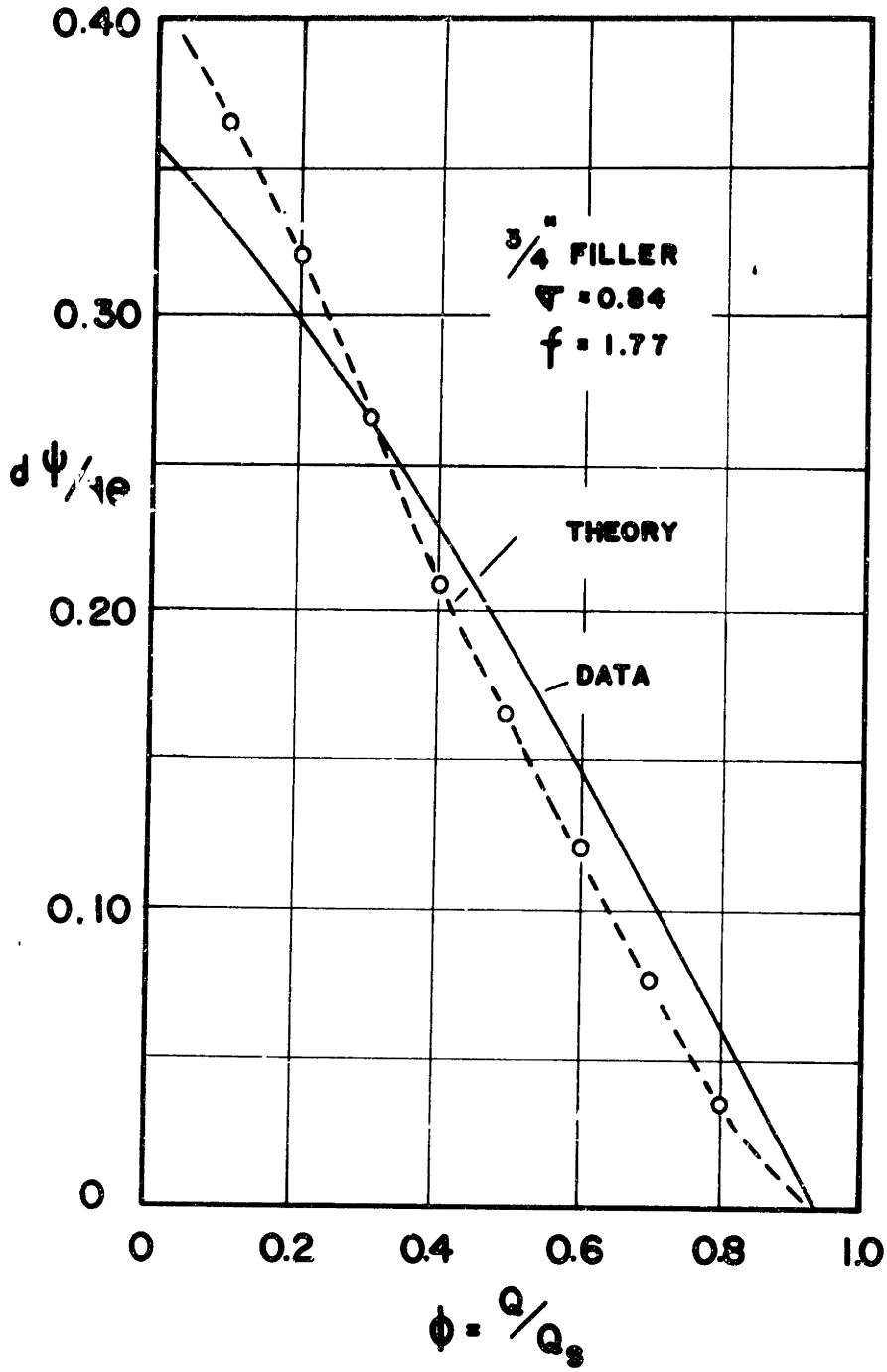

'FRICTION FACTOR' THEORY RESULTS

FIGURE 16

CONTENTS OF APPENDIX

TABLE I

CONSTANTS USED IN ANALYSIS

	No Filler	3/4" Filler	1 1/4" Filler
$A(in^2)$	1.54	1.32	0.955
$R_G(in)$	3.87	3.87	3.84
$R_o(in)$	4.45	4.59	4.61
$R_i(in)$	3.20	3.11	2.98
R_i/R_G	0.828	0.803	0.786
R_o/R_i	1.39	1.47	1.54
$B_o(in)$	0.840	0.515	0.285
$B_i(in)$	1.16	0.735	0.465
C_1	1.130	1.235	1.330
C_2	0.885	0.901	0.909
σ	0.820	0.840	0.867
k_c	3.84	4.87	7.75
$Q_s(CFM)$	0.02165N	0.0186N	0.01325N

APPENDIX A-1

DEVELOPMENT OF ANALYTICAL EXPRESSIONS FOR THE LINEAR REGION

With the basic assumptions made in Section 2. 2. 1, the expressions Eq. (1) to (11) are derived here in more detail. The basic control volumes are found in Fig. 5.

A. 1 Operation on Basic Control Volumes

A. 1. 1 Tangential Pressure Rise

Applying angular momentum relations to the channel control volume

$$\int_A P R dA - \int_A (P + \frac{dP}{d\theta} d\theta) R dA - S R_M = \rho Q_c d\theta (\sigma U_0 R_0 - \alpha U_i R_i)$$

where Sr_m denotes the moment of shear forces at the wall

Simplifying and dividing by $R_c A = \int_A R dA$

$$\frac{1}{\rho} \frac{dP}{d\theta} = \frac{Q_c}{R_c A} [\sigma U_0 R_0 - \alpha U_i R_i] - \frac{S R_M}{R_c A \rho} \qquad (1)$$

and the final term is replaced by the tangential flow losses gH_t.

A. 1. 2 Circulatory Flow Losses

Applying the steady flow energy equation to the channel control volume

$$0 = \int_A (u + \frac{du}{d\theta} d\theta + \frac{V_t^2}{2} + \frac{P}{\rho} + \frac{1}{\rho} \frac{dP}{d\theta} d\theta) \rho V_t dA - \int_A (u + \frac{V_t^2}{2} + \frac{P}{\rho}) \rho V_t dA$$

$$+ (u_i + \frac{\alpha^2 U_i^2}{2} + \frac{P_i}{\rho}) \rho Q_c d\theta - (u_0 + \frac{\sigma^2 U_0^2}{2} + \frac{P_0}{\rho}) \rho Q_c d\theta$$

and simplifying according to original assumptions and defining

$$Q = \int_A V_t \, dA$$

$$\frac{du}{d\theta} = -g H_t \qquad \text{tangential losses}$$

$$u_i - u_o = g H_{cc} \qquad \text{circulatory flow losses in channel passage}$$

Substituting Eq. (1) for $\frac{1}{\rho}\frac{dP}{d\theta}$ with the definitions above

$$\frac{P_o - P_i}{\rho} = \frac{\alpha^2 U_i^2 - \sigma U_o^2}{2} + \frac{Q\omega}{R_c A}(\sigma R_o^2 - \alpha R_i^2) + g H_{cc} \qquad (2)$$

A. 1. 3 Work Input

Applying angular momentum relations to the impeller control volume

$$d\tau = \rho Q_c \, d\theta (\sigma U_o R_o - \alpha U_i R_i) + \frac{dP}{d\theta} d\theta R_c A$$

Since $\omega \, dT = dW$

$$\frac{dW}{d\theta} = \rho Q_c \omega^2 (\sigma R_o^2 - \alpha R_i^2) + \frac{dP}{d\theta} R_G \omega A \qquad (3)$$

The last term is recovered as turbine work across the stripper region.

A. 1. 4 Radial Pressure Rise

Applying the steady flow energy equation to the impeller control volume

$$dW = \left(u_o + \frac{\sigma^2 U_o^2}{2} + \frac{P_o}{\rho}\right)\rho Q_c \, d\theta - \left(u_i + \frac{\alpha^2 U_i^2}{2} + \frac{P_i}{\rho}\right)\rho Q_c \, d\theta + \rho R_c A \left(\frac{1}{\rho}\frac{dP}{d\theta} d\theta\right)\omega$$

simplify by assuming $u_o - u_i \quad gH_{CI}$ and substitute Eq. (3) and (1) for dW and $\frac{1}{\rho}\frac{dP}{d\theta}$:

$$\frac{P_o - P_i}{\rho} = \sigma u_o^2 - \alpha u_i^2 + \frac{\alpha^2 u_i^2}{2} + \frac{\sigma^2 u_o^2}{2} - g H_{ci} \tag{4}$$

A. 2 Assume Expression for Circulatory Losses

The two circulatory flow losses are blade entrance and resistance losses evaluated as:

$$g H_c = \frac{(1-\alpha)^2 u_i^2}{2} + k_c \left(\frac{Q_c}{R_i B_i} \right)^2 \tag{8}$$

By equating Eq. (4) and (2) and solving for gH_C :

$$g H_c = (\sigma u_o^2 - \alpha u_i^2)\left(1 - \frac{Q}{R_c A w}\right) \tag{5}$$

Equate the two expressions for gH_C and solve for Q_c :

$$Q_c = \frac{R_i B_i}{\sqrt{k_c}} \sqrt{(\sigma u_o^2 - \alpha u_i)\left(1 - \frac{Q}{R_c A w}\right) - \frac{(1-\alpha)^2 u_i^2}{2}} \tag{9}$$

A. 3 Dimensionless Performance Expressions

A. 3. 1 Through-Flow

The flow rate or capacity is defined as

$$Q = \int_A V_z \, dA = \frac{\sigma u_o + \alpha u_i}{2} A$$

assuming a linear variation of velocity across the channel. Divide by Q_s :

$$\varphi = \frac{1}{2}\left[\frac{R_o}{R_c}\sigma + \frac{R_i}{R_c}\alpha \right] \tag{12}$$

A. 3. 2 Circulatory Flow

Dividing Eq. (10) by Q_s:

$$\frac{Q_c}{Q_s} = \frac{R_1 B_1}{A} \sqrt{\frac{2}{k_c}} \sqrt{\frac{R_1}{R_0}} \sqrt{(C_1-\varphi)(1-\varphi) - \frac{R_c}{R_1}(C_2-\varphi)^2} \qquad (13)$$

where $C_1 = \frac{R_0^2}{2R_1 R_c}\left(1+\frac{R_1}{R_0}\right)\tau \qquad C_2 = \frac{R_1}{2R_c}\left(1+\frac{R_0}{R_1}\tau\right)$

A. 3. 3 Head Rise, Pressure Coefficient

Divide Eq. (1) by $\omega^2 D^2$ (assume $D \simeq 2r_G$) and simplify

$$\frac{d\psi}{d\theta} = \frac{1}{2}\,\frac{R_1}{R_c}\,\frac{Q_c}{Q_s}\,(C_1-\varphi) \qquad (14)$$

APPENDIX A-2

LEAKAGE CORRECTION ANALYSIS

There are three types of leakage which might occur in the experimental unit tested:

(1) Due to variation of pressure with angular distance from the inlet, there exists a pressure differential capable of causing flow through the clearance between casing and impeller face.

(2) At one end of the stripper region, the pressure is that of the inlet and the other end is the high pressure discharge side. This differential causes flow through the clearance between blades (and fillers) and stripper.

(3) The radial seals are subject to a linear variation of pressure with the differential greatest near the discharge end.

At "shut-off" - when the control valve was shut - there was a net flow measured by the venturi tube. This leakage was attributed to the radial seals. In order to correct the experimental head curve the following analysis was performed.

$$\varphi_{loc} = \varphi_M - \int_0^{\theta} \varphi_l \, d\theta$$

where φ_{loc} flow at the point considered

φ_M flow measured by venturi

φ_l leakage flow/radian at any point

θ angle measured from inlet

Leakage is assumed proportional to the square root of the head at any point. $\varphi_L = K_3 \sqrt{\psi}$

The head varies linearly:

$$\psi = \left(\frac{\psi}{\theta}\right)_0 \theta \qquad \text{where } \left(\frac{\psi}{\theta}\right)_0 : \text{gradient at exit}$$

$$\therefore \varphi_L = K_3 K_4^{\frac{1}{2}} \sqrt{\theta} \qquad \text{where } K_3 = \left(\frac{\psi}{\theta}\right)_0$$

Substituting this variation and integrating:

$$\varphi_{Loc} = \varphi_M - \int_0^{\theta} K_3 K_4^{1/2} \theta^{1/2} d\theta = \varphi_M - K_3 K_4^{1/2} \frac{2}{3} \theta^{3/2}$$

Using a boundary condition: $\theta = \theta_0 \quad \varphi_{Loc} = \varphi_{EXIT}$

$$[\varphi_M - \varphi_{EXIT}]' = K_3 K_4^{1/2} \frac{2}{3} \theta^{3/2}$$

or

$$\varphi_{Loc} = \varphi_M - [\varphi_M - \varphi_{EXIT}]' \left(\frac{\theta}{\theta_0}\right)^{3/2}$$

Integrate to find an average value:

$$\bar{\varphi}_{Loc} = \frac{1}{\theta_0} \int_0^{\theta_0} \left(\varphi_M - [\varphi_M - \varphi_{EXIT}]' \left(\frac{\theta}{\theta_0}\right)^{3/2}\right) d\theta$$

$$\bar{\varphi} = \bar{\varphi}_M - \frac{2}{5} [\varphi_M - \varphi_{EXIT}]'$$

The average leakage flow is found by integrating:

$$\bar{\varphi}_L = \int_0^{\theta} \varphi_L d\theta = K_3 \left(\frac{\psi}{\theta}\right)_0^{1/2} \int_0^{\theta_0} \theta^{1/2} d\theta = K_3 \left(\frac{\psi}{\theta}\right)_0 \frac{2}{3} \theta_0^{3/2}$$

at "shut-off" the average leakage flow has been measured.

$$\varphi_L = K_3 \left(\frac{\psi}{\theta}\right)_0' \frac{2}{3} Q^{3/2} \qquad \text{where } \left(\frac{\psi}{\theta}\right)_0' \text{ exit pressure gradient at "shut-off"}$$

Dividing $\frac{\bar{\varphi}_2}{\bar{\varphi}_2'} = \sqrt{\frac{\psi}{\psi'}}$

and the application formula appears:

$$\bar{\varphi}_2 = \bar{\varphi}_2' \sqrt{\psi/\psi'}$$

where $\varphi_2' = \frac{2}{5}\varphi_M'$ φ_M' measured when $\varphi_{exit} = 0$

This was the only correction applied to the head curves of the three pump configurations. Corrections for internal leakage, types (1) and (2), have been made on previous units with little effect on the head curves.

APPENDIX A-3

'FRICTION FACTOR' ANALYSIS

The geometry of the "torus" pump is very similar to the ordinary fluid coupling. The fluid coupling has two rotating impellers at slightly different speeds. The fluid within the coupling flows helically and circulates in one passage and then comes over to the opposite impeller passage.

Wislicenius[3] evaluates the circulatory flow losses by this expression

$$gH_c = f \frac{V_m U}{2}$$

where f = a friction factor which remains almost constant in the range of 0.46 - 0.48

V_m = mean velocity of circulatory flow

U = average wheel speed.

There is a shock loss due to the relative velocity between the two wheels, but in the fluid coupling this loss is quite negligible. At a slip of 10% shock loss is 4.9% and at slip of 1% shock loss is 0.49%.

A "friction factor theory" based upon Wislicenius' "f" plus the shock losses leads to an expression for circulatory flow head loss

$$gH_c = \frac{(1-a)^2 U_1^2}{2} + f \frac{Q_c}{R_i B_i} (\omega R_c)$$

This expression was used with the theoretical Eq. (5) to give:

$$\frac{d\psi}{d\theta} = 2 \frac{R_i B_i}{A} \frac{1}{f} \left(\frac{R_i}{R_c}\right)^2 (C_1 - \psi) \left[(C_1 - \psi)(1-\psi) - \frac{R_c}{R_i} (C_2 - \psi)^2 \right]$$

where C_1 and C_2 have been previously defined.

This expression for the head coefficient is the same as the circulatory flow theory expression, Eq. (13) & (14), with the exception of the final term which should be to the half power. Mathematically, this means the "friction factor theory" head curve will have greater curvature than the circulatory flow theory head curve. Fig. 12 shows the match between theory and data. The values of f and ¶ are determined in the same manner as k_c and ¶, Section 5.2.1.

The poor match may be attributed to Wislicenius' expression. From the results, it can be concluded that although the flows in the fluid coupling and regenerative pump are circulatory, they are not comparable machines. The value of f for the pump was four times greater and not constant for any of the configurations denoting the pump flow losses are much more severe.

PHOTOGRAPHS

1. VIEW OF APPARATUS INCLUDING INSTRUMENTATION, UNIT, AND DYNAMOMETER.

2. VIEW OF CASING AND IMPELLER WITH 1 1/4" FILLER INSTALLED.

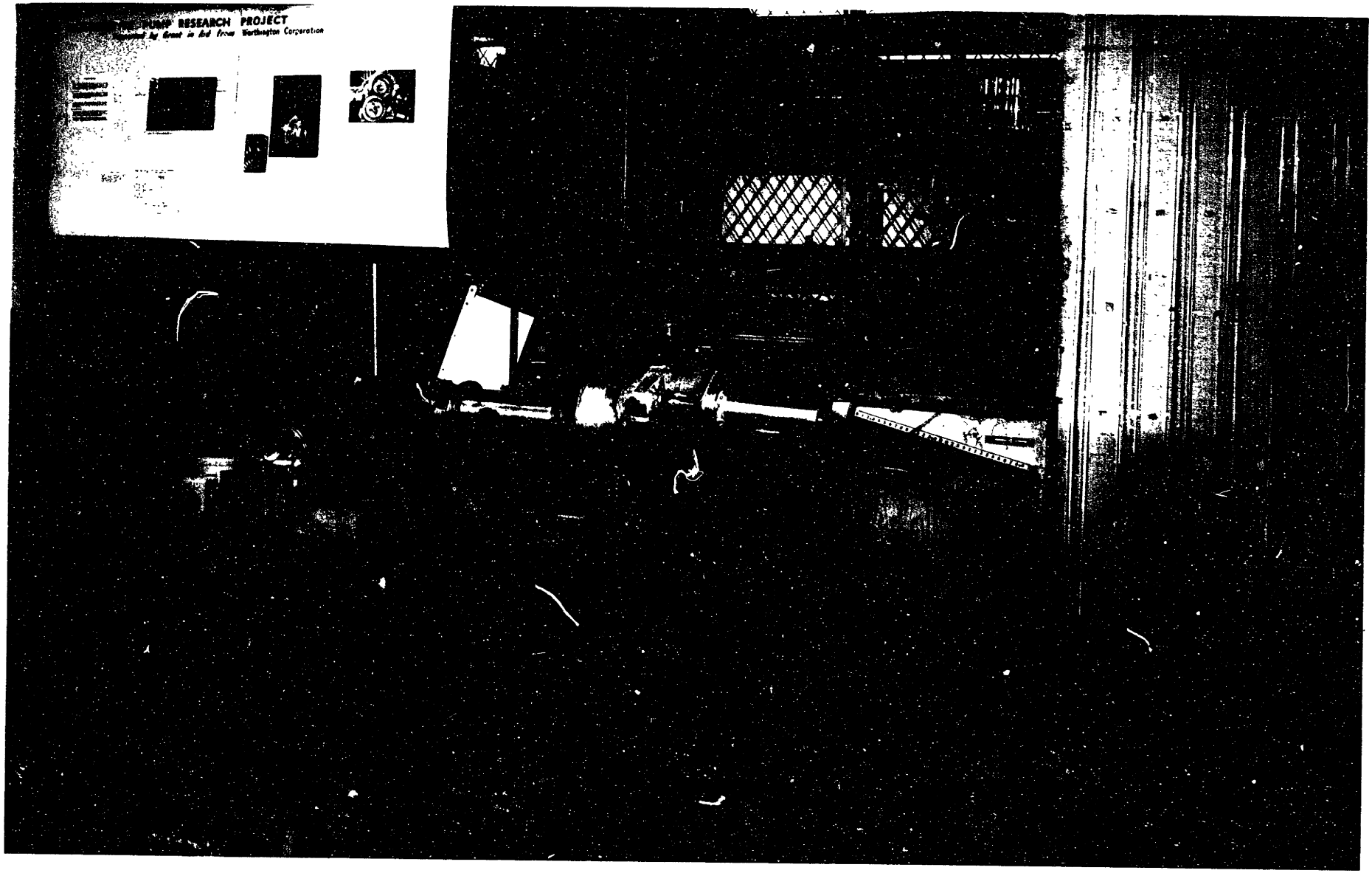
RESEARCH PROJECT
Worthington Corporation

BIBLIOGRAPHY

1. Santalo, M. A., "Experimental Investigation of Variables Affecting Regenerative Pump Performance". S.M. Thesis, M.I.T., June 1954.

2. "A Comparison of Regenerative Pump Theories Supported by New Performance Data". Y. Senoo, A.S.M.E. Paper No. 55-SA-44.

3. Fluid Mechanics of Turbomachinery, G. F. Wislicenius, McGraw-Hill, 1947.

4. Performance Chart of Sta-Rite Pumps.

5. "A Theory of the Fluid-Dynamic Mechanism of Regenerative Pumps", by W. A. Wilson, M. A. Santalo, and J. A. Oelrich, A.S.M.E. Transactions, Volume 77, November 1955, pp. 1303-1311.

6. Centrifugal Pumps, Turbines, and Propellors, Spannhake, Technology Press, M.I.T., 1934.

7. Centrifugal and Rotodynamic Pumps, Addison, H., pp. 155-157.

8. "Theoretical and Experimental Analysis of a Regenerative Turbine Pump", Hopkins, T. and Lazo, L. Senior Thesis, M.I.T., January 1953.

9. "Experimental Investigation of the Pressure Distribution in a Regenerative Pump, The Sta-Rite TH-7", Lutz, G. F. Senior Thesis, M.I.T., May 1953.